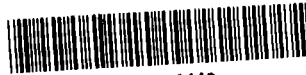


WA. 6609/7-01.7(3)

PETROGENESIS AND STRUCTURAL & TH

POWELL/SNYDER/CHURCH 1 1983

G110 14 DB/ 21



NR01592442

7

**PETROGENESIS
AND
STRUCTURAL & THERMAL HISTORY
OF CORE FROM
TRAENABANKEN 6609/7-1 WELL:
FINAL REPORT**

**B. N. POWELL
W. S. SNYDER
R. K. CHURCHILL**



January 19, 1983

INTER-OFFICE CORRESPONDENCE / SUBJECT:

Characterization of Cores from
Traenabanken 6609/7-1 Well

FILE: BNP-2-84
WSS-1-84
RKC-2-84

TO: D. A. Morris (r) I. A. Knight
E&P Group
Stavanger, Norway

FROM: B. N. Powell
237 GB, Ext. 9664
W. S. Snyder
252 GB, Ext. 9703
R. K. Churchill
241 GB, Ext. 9666

In response to your request to determine the petrogenesis and structural and thermal history of two short cores from the Traenabanken 6609/7-1 well, we submit this final report. It is our understanding that the principal benefit derived from this well will be information, and that data bearing on the Traenabanken thermal history are of particular interest.

This final report is an expanded version of our preliminary report issued December 6, 1983 (BNP-3-83, WSS-1-83). Added are analytical data (microprobe analyses; fluid inclusion measurements), numerous photomicrographs and some additional discussion. A section on phase chemistry has been added, and the sections on structural history and fluid inclusions are much expanded. The fundamental interpretations, conclusions, and recommendations have not changed, however, and much of the earlier text is incorporated.

Summary of General Features

Analyses of hand specimens and 15 polished thin sections from both cores, plus 3 fluid inclusion sections reveal several general features, summarized below.

1. The basic lithology is a muscovite-bearing quartzo-feldspathic schist and is the product of regional metamorphism.
2. The principal metamorphic assemblage is quartz + K-feldspar + muscovite with variable amounts of calcite. Accessory phases (doubtless inherited from the sedimentary precursor, a siltstone) include tourmaline, zircon, rutile, pyrite and apatite. Late-stage (post-metamorphic) alteration minerals include kaolinite (after muscovite) and calcite (vein-filling).
3. Mineral assemblages, textures and the uniformity of phase compositions (determined by electron microprobe) attest to general metamorphic equilibrium over the scale of the two cores.

FILE: BNP-2-84

WSS-1-84

RKC-2-84

4. Metamorphic recrystallization was syntectonic as evidenced by subparallelism between metamorphic foliation and the axial surfaces of microfolds.
5. The style of the principal deformational phase and the general metamorphic fabric are consistent with Caledonian tectonism. [This is conjectural, however, as the sampled lithology is not suitable for meaningful geochronologic determinations. (See item 12 below and later text.)]
6. Metamorphic facies - never rigorously definable on the basis of a single lithology - is difficult in this case to reliably estimate from the mineralogy of the rock: the assemblage quartz-muscovite-potassium feldspar-calcite is stable throughout both the greenschist and amphibolite facies.
7. The phase chemistry of feldspar and muscovite is consistent with formation under moderate metamorphic conditions. Muscovite compositions, in particular, suggest crystallization temperatures in a range generally associated with the upper greenschist or lower amphibolite facies of regional metamorphism.
8. Tectonism following metamorphic recrystallization produced early microfractures and later calcite-cemented veins and breccias; the local alteration of muscovite to kaolinite occurred at this stage. These events could have occurred soon after or much later than the principal episode of metamorphism/tectonism.
9. Minimum formation temperatures of late- or post-metamorphic secondary fluid inclusions in matrix quartz are in the range 180-226°C. Pressure corrections could raise this range by 50°C or more.
10. Pressure-corrected formation temperatures of fluid inclusions in two types of late-stage vein calcite fall in the range 114-145°C.
11. Inclusion fluids in vein calcite are CaCl₂-NaCl brines with salinities higher than that of seawater. A hydrocarbon (?) liquid was observed in one calcite fluid inclusion.
12. The given metamorphic mineral assemblage, coupled with abundant evidence for post-metamorphic veining and hydrothermal alteration, indicates that any geochronologic determinations would have little, if any, reliability or meaning. The rock has not behaved as a closed system and has experienced a number of tectonic events.

In answer to two specific questions raised by Ian Knight (telephone conversation with D. W. Rhett, 11/17/83), we make the following observations/interpretations:

13. The mineral(s) responsible for the greenish coloration, about which you inquired, is probably muscovite, as the latter exhibits a pale green pleochroism in thin section. Some chlorite (?) and/or epidote may be present locally on slickensided fracture surfaces.
14. The breccia at the top of the core is of tectonic origin.

FILE: BNP-2-84

WSS-1-84

RKC-2-84

In the following paragraphs we present evidence and observations leading to the above conclusions.

Petrology

The basic metamorphic assemblage quartz, K-feldspar, muscovite, and calcite is present in all 15 thin sections prepared (from both cores), although the relative abundances of the phases are variable from section to section and within a given section. Despite the fact that the mineralogy of the rock changed little during metamorphism (aside from the reconstitution of precursor clays to muscovite), the textural features indicate complete recrystallization. In fact, the most strikingly metamorphic aspect of the rock is its fabric, which is markedly schistose (Figures 1-3).

As illustrated in Figures 1 and 3, the foliation is defined by a strong subparallelism of elongate grains of quartz and feldspar and by alignment of muscovite flakes. The latter occur more or less dispersed throughout the quartzo-feldspathic matrix and also are locally concentrated in thin layers probably reflecting argillaceous laminae in the original siltstone. Clearly, the rock was recrystallized within a stress field (syntectonically): even in mica-deficient areas the schistosity is very pronounced due to the elongated morphology and strongly preferred orientation of quartz and feldspar grains. The intricate sutured grain boundaries (Figures 1b and 3b) offer further evidence for crystalloblastic (metamorphic) crystallization.

The feldspar grains are invariably untwinned, a characteristic of low to moderate grade metamorphic feldspars. [The distinction between microcline and orthoclase thus becomes most difficult, further complicating facies estimate.] All the feldspars are very potassium-rich: no discrete plagioclase (including albite) has been identified petrographically or with the microprobe.

Quartz typically shows evidence of strain in the pronounced undulose extinction (ubiquitous) and presence of deformation lamellae (less common). Numerous trails of minute fluid inclusions outline healed microfractures which must have formed after the metamorphic recrystallization (see below under "Structural Chronology").

Calcite in the rock exhibits two basic parageneses. It occurs locally as disseminated, typically turbid, masses within the basic rock matrix, and as such, evidently represents in situ recrystallization from precursor carbonate in the original siltstone. Calcite also occurs in veinlets and breccia zones which characteristically cross-cut the foliation and represent a late-stage (i.e. post-metamorphic) hydrothermal event. Many of these vein systems are decorated with thin films of orange-brown, non-descript material. The latter is probably hydrated iron oxide(s) ("limonite") formed from oxidation of pyrite. Some of the wider vein systems contain rotated, angular clasts of the basic schistose lithology enclosed in a matrix of coarsely crystalline (sparry) calcite (Figure 2).

Phase Chemistry

In concert with the petrographic features described above, the phase chemistry of feldspar and mica are indicative of metamorphic equilibration under moderate conditions. Over 125 quantitative electron microprobe analyses in 8 thin sections from both cores are summarized in Tables 1-4. To conserve

FILE: BNP-2-84
WSS-1-84
RKC-2-84

space, ranges and averages are given in Tables 1-4 rather than a complete tabulation of all analysis. [The latter can be provided, of course, if required.]

One important general feature of the microprobe data is the very small degree of compositional variation. Grain-to-grain variation within a section is similar in magnitude to the variation of the average from section to section. Significantly, no appreciable intragranular variations were detected.

The feldspars are uniformly very Ca-deficient (even for alkali feldspars). They are also very K-rich, exhibiting a total range of albite content of only 1.5-11.8 mol. %. No perthitic intergrowths of Na-rich and K-rich feldspars were detected. These features, together with the absence of any twinning, are collectively consistent with metamorphic re-equilibration at moderate temperatures. Although texturally recrystallized and chemically re-equilibrated during metamorphism, the feldspars must have formed from precursor (detrital or authigenic) feldspar in the original siltstone, however, because in feldspar-free argillaceous rocks, K-feldspar forms at the expense of phyllosilicates only under "high-grade" conditions (upper amphibolite facies or higher) of the "sillimanite zone".

The mica compositions give a better indication of metamorphic grade and, hence, are worthy of more discussion. The composition of "white mica" in metamorphic rocks varies with temperature and pressure of formation. Empirical observations based on naturally occurring micas from numerous localities representing a range of metamorphic "grade" consistently indicate that in lower grade rocks the stable white mica is a "phengitic muscovite", characteristically having a high Si content. The substitution of Si^{+4} for Al^{+3} is balanced by substitution of Mg and Fe for Al in octahedral sites in the crystal lattice (Deer, et al., 1962).

As metamorphic grade increases the Si content of equilibrium muscovite drops, reaching the ideal muscovite formula near the upper limit of muscovite stability (Greenwood, 1976). The dependence of muscovite Si content on temperature and pressure is indicated in Figure 4. For the purpose of comparing the Traenabanken muscovites to those from other metamorphic terranes, selected analyses encompassing the range and average are shown in Table 5, along with the compositions of ideal muscovite. Also listed are muscovites from the low grade Otago (New Zealand) greenschist terrane and a medium-grade, garnet-mica schist from Scotland. Clearly, the Traenabanken muscovites, on average, more nearly approach ideal muscovite than they do the phengitic micas from New Zealand. This is particularly evident when the respective Si contents (from the lower half of Table 5) are compared to Figure 4.

The Traenabanken muscovite chemistry is consistent with equilibrium under moderate metamorphic conditions, perhaps similar to those typical of the upper greenschist or even the lower amphibolite facies. Figure 4, however, cannot be used to derive a quantitative temperature estimate for Traenabanken metamorphism, because we cannot assess the other factors which influence the muscovite equilibrium composition, including such things as pressure and fluorine activity. Nonetheless, the mica phase chemistry does clearly indicate formation of the basic Traenabanken lithology under true metamorphic conditions and supports the conclusions drawn from petrographic evidence regarding the style of metamorphism and the attainment of approximate metamorphic equilibrium.

FILE: BNP-2-84

WSS-1-84

RKC-2-84

Temperatures of post-metamorphic events can be quantitatively estimated, however, from fluid inclusion data (see below). Such temperatures clearly are lower than peak metamorphic temperatures, and the highest estimates (from inclusion data) could be used as a lower limit for the principal metamorphism.

Identification of the low-temperature, late-stage alteration product of muscovite as kaolinite was confirmed by microprobe analysis. The analyzed composition is typical of true kaolinite: SiO₂ (45.4 wt.%), Al₂O₃ (40.1), TiO₂ (0.04), "FeO" (0.07), MgO (0.00), CaO (0.04), K₂O (0.10), Na₂O (0.00), sum (85.8) (balance H₂O).

Alteration

Germane to any considerations of geochronologic determinations or stable isotope studies is the important petrographic evidence that, despite a general attainment of metamorphic equilibrium, the rocks have not behaved as a closed system, and many individual mineral grains show evidence of lower temperature, hydrothermal alteration. At least two fracturing events (chronicled below), each accompanied by fluid movement through the rocks, are evident. Partial local alteration of muscovite to kaolinite (with consequent mobilization of potassium) occurred during at least one of these events. (See Figure 3.)

Structural Chronology

Structural features visible in hand specimen and thin section reveal at least three phases of deformation, as outlined below.

Phase 1: Development of tight to isoclinal similar folds, contemporaneous with metamorphism. The metamorphic foliation parallels the axial planes of these folds.

Phase 2: Development of a conjugate set of fractures at roughly 60° to the metamorphic foliation and of another set at about 90° to the foliation. During this deformational phase microstylolites developed subparallel to metamorphic layering. Trains of fluid inclusions associated with microcracks and with the tips of the pillars and sockets of the microstylolites probably represent healed microfractures developed during this phase of deformation.

Phase 3: Formation of veins and dilation breccias, cemented with sparry calcite. Alteration of muscovite to kaolinite probably occurred during this phase.

Structures: Discussion

The parallelism of the metamorphic foliation and axial planes of the similar folds implies that Phase 1 structures developed during a period of layer-parallel compressive stresses, and of elevated temperatures capable of producing complete metamorphic recrystallization. A major orogenic event, such as the Caledonian orogeny, could account for these structural features. Figure 5 shows examples of the folds in a polished core chip (a) and in thin section (b).

Tectonic Breccia

Hand specimen examination of the breccia present in the top of Core 1 (1944.24m) points compellingly to a tectonic origin, as evidenced by the features outlined below.

1. The fragments are notably angular (Figure 11a, b).
2. Clasts are in various stages of disaggregation (Figure 11b).
3. Narrow zones of very finely comminuted material cross-cut the entire segment of core (~30 cm) and frequently contain chlorite (?) and/or epidote, suggesting intense cataclasis and associated alteration (Figure 11a, b).
4. Slickensides are visible on exposed surfaces of these fine-grained zones (Figure 11c).
5. Angular fragments separated by finer-grained material can be fitted together to reconstruct larger clasts (Figure 11b).

These observations are only consistent with in situ brecciation through tectonic processes. The rock is not a sedimentary breccia or conglomerate. The brecciation probably developed during deformational Phase 3 (see above), although the data do not preclude an even younger (4th) deformational event. In any case, this brecciation is clearly one of the younger features visible in the core.

Geochronology: Recommendations

Unfortunately, the lithology exhibited by the materials forwarded to us for characterization (Core 1, 1944.24-1946.0m and Core 2, 1968-1969m) is not suitable for meaningful radiogenic "age" determinations. Reliable Rb-Sr geochronology requires, among other things, the presence of at least three cleanly separable mineral phases representing K-(Rb-) rich and Ca-(Sr-) rich compositions. Of the two potassium-rich minerals present in this rock, one (muscovite) is variably altered by post-metamorphic, open-system, chemical reaction(s). Suitable Ca-rich phases are not present: although some of the calcite may be "metamorphic", much of it is of a late-stage lower temperature origin. The only other Ca-rich mineral identified is apatite, and it is present in minute grains (5-20 μ m) in exceedingly low abundance (<<1%) and sporadic distribution. A reliable initial Sr^{87}/Sr^{86} ratio cannot be assumed, and thus an adequate isochron cannot be defined to provide any meaningful interpretation. The multiple phases of deformation and the alteration also preclude useful K-Ar determinations.

Quite aside from the mineralogical stumbling blocks, the very fine-grained nature of the rocks coupled with the exceedingly intricate, sutured, grain boundaries would make it practically impossible to provide the quantitatively clean mineral separations necessary for reliable radiogenic (or stable) isotope studies. Also, the separation of early (metamorphic) from late (hydrothermal) calcite and of fresh from partly kaolinized muscovite would not be possible.

As a result of these considerations, at this stage we recommend against attempting any radiogenic or stable isotopic analysis of these materials.

FILE: BNP-2-84

WSS-1-84

RKC-2-84

Information useful for thermal modeling will have to be derived from other investigations. Of course, if sufficiently different lithologies become available, the applicability of some of these techniques could be re-evaluated.

Fluid Inclusions

Fluid inclusions occur in vein calcite and in matrix quartz. Both occurrences are 2-phase, liquid-vapor inclusions (liquid dominant) and contain no daughter minerals. Inclusions in the quartz are "secondary", and were formed by fluid trapped in healed microfractures. These secondary inclusions are very small (mostly $< 2\mu\text{m}$) and form lines or "trains" that are continuous across grain boundaries (Figure 12). The trains typically cross-cut the metamorphic fabric, but do not continue into the vein calcite. Consequently, they must have formed during a late (post-metamorphic) fracturing event (Phase 2 discussed above).

Vein calcite is of two types, distinguished in part by the fluid inclusions. Type 1 is dark and mottled in thin section and contains numerous solid and fluid inclusions (Figure 13a, b). Type 2 calcite is clear, more coarsely crystalline, and contains fewer fluid inclusions and only rare solid inclusions (Figure 13a, c). Type 1 calcite occurs typically along the sides of veins, while Type 2 occupies vein interiors. Boundaries between the two are narrow and transitional. Type 1 was probably deposited before Type 2, but with no hiatus between the two. Both types also occur in breccia zones adjacent to the vein, but the spatial relationships outlined above are less consistent here. Fluid inclusions in both calcite types are mostly primary, i.e., they were trapped during calcite formation. Thus, the inclusions represent T, P and fluid compositions at that time.

Homogenization temperatures (the minimum temperatures of fluid entrapment), $T(h)$, for the secondary inclusions in matrix quartz range from 180-226°C (six determinations). [Homogenization temperature is what is measured on the heating stage of the microscope. The "true" temperature of inclusion formation requires a correction for pressure effects.] The small size of these inclusions makes $T(h)$ measurements difficult and precludes determination of fluid composition and salinity. The latter parameters are required to estimate the "true" temperature of inclusion formation. The indicated minimum temperatures of 180-226°C would be consistent with microfracturing and fluid entrapment either during the waning stages of regional metamorphism or during a later (separate) event. Temperature corrections could reasonably raise the indicated values by 50°C, or more.

Homogenization temperatures for inclusions in Type 1 calcite range from 93.2-101°C (average 96.0°C for 3 measurements). The $T(h)$ for inclusions in Type 2 calcite averages 99.8°C (6 measurements), with a range of 91-110°C. Statistically, $T(h)$ for the two sets of inclusions are essentially indistinguishable.

Fluid compositions can be estimated from measurements of "first melting" of the fluid inclusions (done on a cooling stage). Five such determinations indicate that fluids in both calcite types are aqueous and contain at least one dissolved salt (probably CaCl_2) in addition to NaCl . Slight differences in first melting temperatures between Type 1 calcite inclusions ($\sim 25^\circ\text{C}$) and Type 2 inclusions ($\sim 31^\circ\text{C}$) imply different $\text{NaCl}:\text{CaCl}_2$ ratios in the trapped fluids and a slight change in fluid chemistry with time during vein filling.

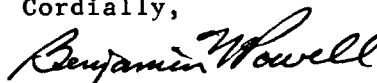
Salinities were estimated for five fluid inclusions in calcite and the values (in equivalent wt. % NaCl) are: 4.9 (Type 1); and 3.2, 4.3, 4.8, and 9.5 (Type 2). The 9.5 percent estimate is from an inclusion near the boundary between the two calcite types. With the one exception, all are in excess of the salinity of seawater (3.5%).

Based upon fluid compositions and assumptions that: 1) the vein calcite in this core sample was deposited at about its present depth (~1900m below sea level); and 2) the average density of the overburden is 2.0-2.5 g/cc, the pressure correction for the formation temperatures of vein calcite inclusions is probably 20-30°C. Thus, the actual temperatures of vein calcite formation would lie in the range 114-145°C, and are distinctly different from the temperatures for secondary inclusions in the matrix quartz. With better information on thickness and average density of the overlying lithology, plus information on regional tectonic history, a better estimate of this temperature correction might be possible.

One inclusion found in Type 2 calcite contains a dark colored liquid, possibly a hydrocarbon (Figures 13a and 14a), although it exhibited no ultraviolet fluorescence. The inclusion apparently homogenized on heating (Figure 14), but no other information could be obtained. The presence of this inclusion suggests that at least minor amounts of organics were transported by fluids associated with Type 2 calcite.

We hope this report will answer most of your questions and needs. It is unfortunate the lithology of the cores is not more amenable to isotope studies — especially radiogenic age determinations — but then Mother Nature doesn't always cooperate! Please let us know if we can provide any further information, specific or general. To facilitate any further inquiries you may have about this report, the areas of principal responsibility of the three authors are as follows: BNP [Petrology; Phase Chemistry; Alteration; Geochronology; Recommendations]; WSS [Structural Chronology; Structures: Discussion; Tectonic Breccia]; RKC [Fluid Inclusions].

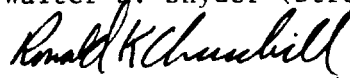
Cordially,



Benjamin N. Powell (Petrologist)



Walter S. Snyder (Structural Geologist)



Ronald K. Churchill (Geochemist)

BNP/WSS/RKC/laf

Attachments

cc: R&D Records

N. L. Burnett (r) M. N. McElroy

D. W. Rhett

H. A. Kuehnert

January 16, 1984

FILE: BNP-2-84

WSS-1-84

RKC-2-84

A-1

Figure 1. General fabric of regional metamorphic quartz-muscovite-feldspar schist from Traenabanken 6609/7-1 well. Foliation is defined by preferred orientation of elongate quartz (dark gray) and potassium feldspar (light gray) grains and of muscovite flakes (medium gray, stippled-looking).

- a) Back-scattered electron scan image (BEI) of polished thin section of sample from Core 1, cut C, section 7. Black areas are pits in the section caused by plucking. A muscovite-rich layer is visible running horizontally across the approximate middle of the photograph. The foliation is especially visible in this low magnification picture. (Narrow dimension of field is 2.25 mm.) (40X magnification.)
- b) BEI of polished thin section from Core 1, cut C, section 2, at higher magnification (100X). Note schistosity and pronounced crystalloblastic texture characterized by intricate sutured grain boundaries, especially between quartz (dark gray) and K-feldspar (light gray, labeled "K"). Muscovite flakes are also present (intermediate gray, labeled "m"). Scale bar is 100 μm .

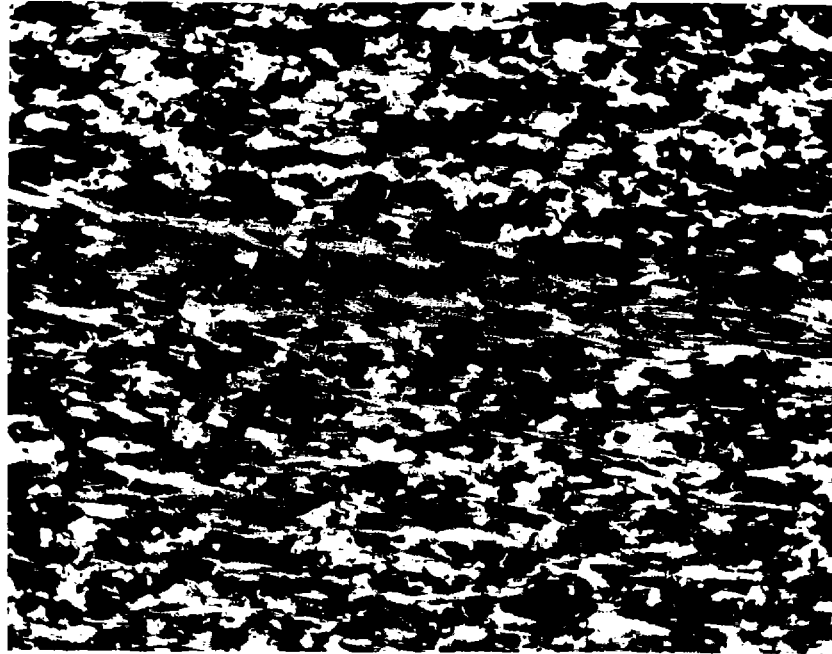


Figure 1a

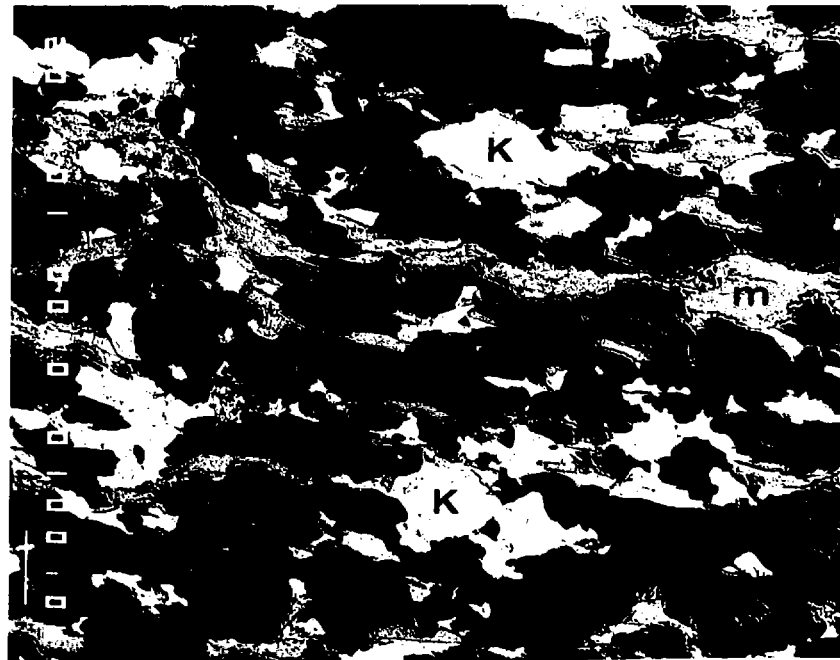


Figure 1b

Figure 2. BEI of polished thin section of sample from Core 1, cut C, section 5, Traenabanken 6609/7-1 well, showing rotated angular breccia clasts of quartz-mica-feldspar schist lithology in matrix of coarse sparry calcite (lightest gray, labeled "C"). The misorientation of the metamorphic fabric visible in the two largest clasts attests to rotation. The field of view is a portion of centimeter-wide breccia zone which cross-cuts the foliation of the rock. (Narrow dimension of the field is 2.25 mm.) (40X magnification.)



Figure 2

Figure 3. BEI's of a polished thin section of a sample from Core 1, cut C, section 7, Traenabanken 6609/7-1 well, showing partial replacement of muscovite ("m") by kaolinite (dark bands interlayered with muscovite). Q is quartz, K is potassium feldspar and R is rutile.

- a) 100X magnification. Note abundance of kaolinite replacement in vicinity of microfracture, now partially opened (black band in photograph). Scale bar is 100 μm .
- b) 860X magnification. The dark kaolinite layers in light gray muscovite are readily visible and have been confirmed by microprobe analysis. (Narrow dimension of field is about 100 μm .)

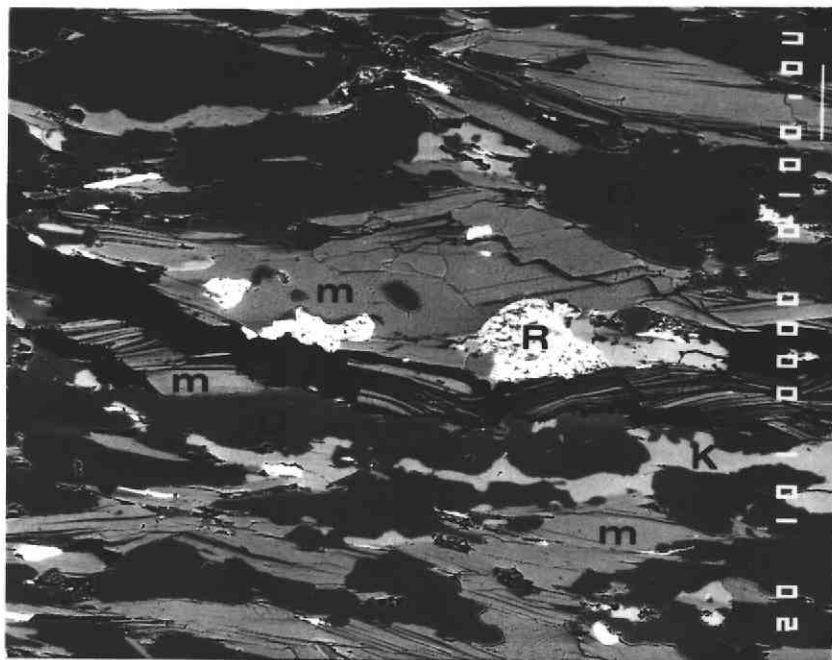


Figure 3a

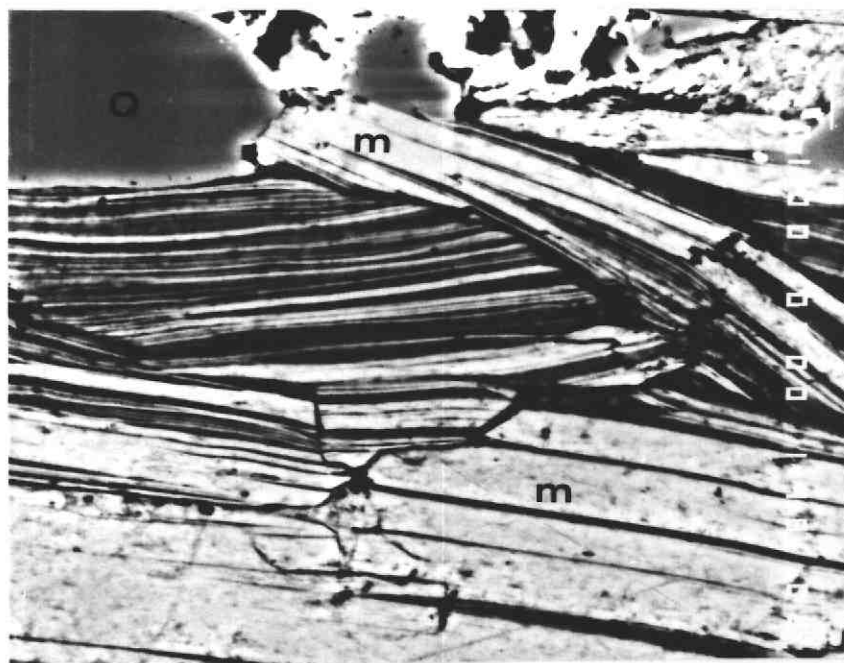


Figure 3b

January 16, 1984

FILE: BNP-2-84

WSS-1-84

RKC-2-84

A-7

Figure 4. Si^{+4} content of phengite-muscovite as a function of temperature and pressure. At a given pressure the Si^{+4} content of muscovite decreases with increasing temperature up to the upper stability of the phase. The highest temperature curve above is the upper stability limit of muscovite in the absence of quartz. In the presence of quartz muscovite breaks down to K-feldspar plus $\text{Al}_2\text{SiO}_5 + \text{H}_2\text{O}$ at somewhat lower temperatures (for a given pressure). Figure modified from Greenwood (1976), Figure 19.

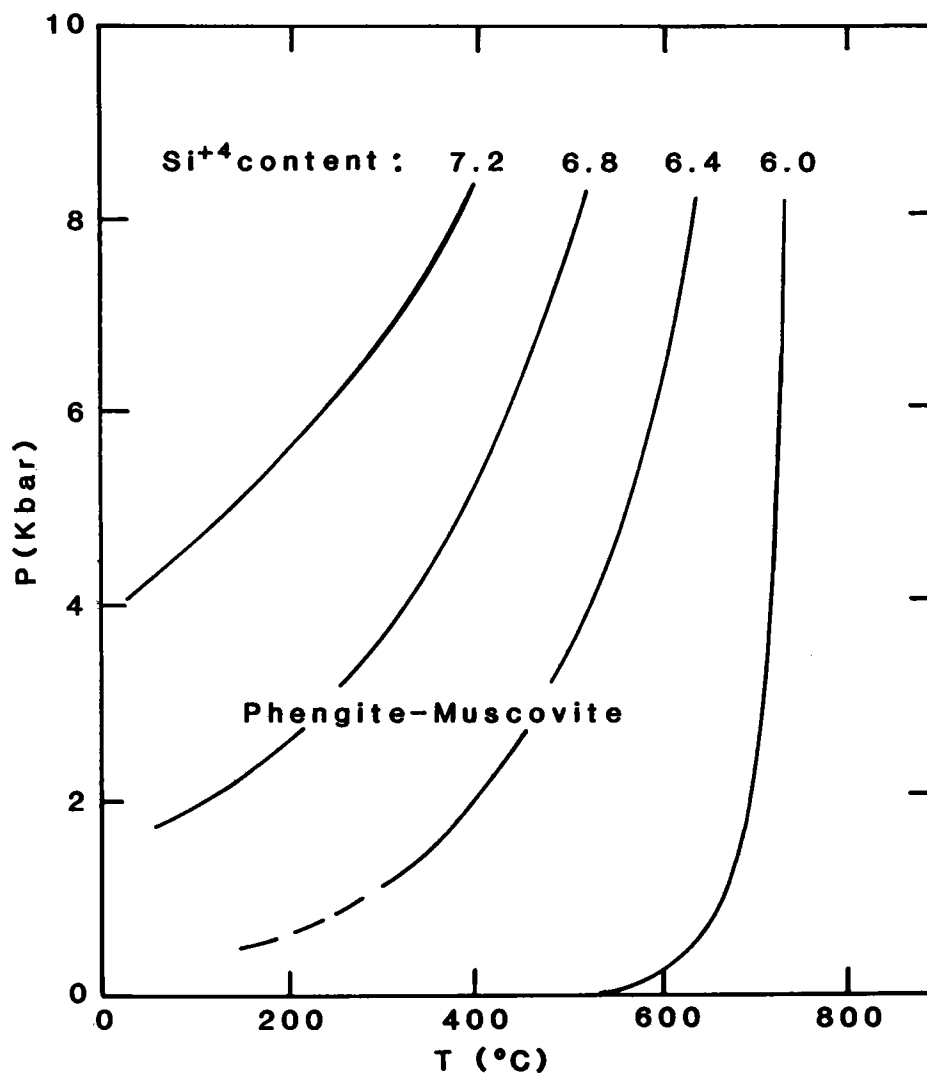


Figure 4

Figure 5. Similar folds in the schist from Traenabanken 6609/7-1 well.

- a) Polished core chip from Core 1, Cut A, Chip 3. The banding is defined by layers that are variably quartz-feldspar and muscovite-rich. A calcite vein cross-cuts these folds and is comprised of a reddish brown, early generation of calcite and a translucent green, second generation. Note how the original form of the folds can be restored by removing the displacement perpendicular to the vein.
- b) Photomicrograph in plane light of upper fold hinge in Figure 5a. The thin section was cut from the facing piece to that in a and the image is therefore reversed. The dark bands are muscovite-rich. The metamorphic foliation is parallel to the axial plane of the fold. The two generations of calcite are separated by a dark band. Long dimension of the photomicrograph is 18mm; from Core 1, Cut A, section 3.



Figure 5a



Figure 5b

Figure 6. Photomicrographs of fractures, veins, and microstylolites within schist from the Traenebanken 6609/7-1 well.

- a) Fracture at 60° to the metamorphic foliation cross-cuts the sample. The central portion of the fracture is a series of right-stepping en echelon microfractures suggesting a component of right-lateral shear.. (Plane light; long dimension of photo is 6mm; Core 1, Cut C, Section 7.)
- b) Conjugate sets of fractures at $60-70^{\circ}$ to the metamorphic foliation (parallel to long dimension of photo). Dilation breccia truncates the fractures at the top. Calcite fills the fracture on the bottom, and partly fills the central fracture. The fracture just below the breccia follows a zone of fluid inclusions. (Plane light; vertical dimension is 18mm; Core 1, Cut C, section 5.)
- c) Microstylolite at the boundary between megaquartz (right) and finer-grained schist (left). Foliation parallels long dimension of photo. The megaquartz may have been a layer of coarser quartz sandstone prior to metamorphism. (Plane light; long dimension of photo is 2.3mm; Core 2, Cut C, section 2.)
- d) Microstylolite developed along a fracture at 60° to the foliation. Foliation is at a slight angle to the short dimension of the photo. Dark streakings perpendicular to the foliation are trains of fluid inclusions. (Plane light; short dimension is 0.55mm; Core 1, Cut C, section 5.)



Figure 6a



Figure 6b

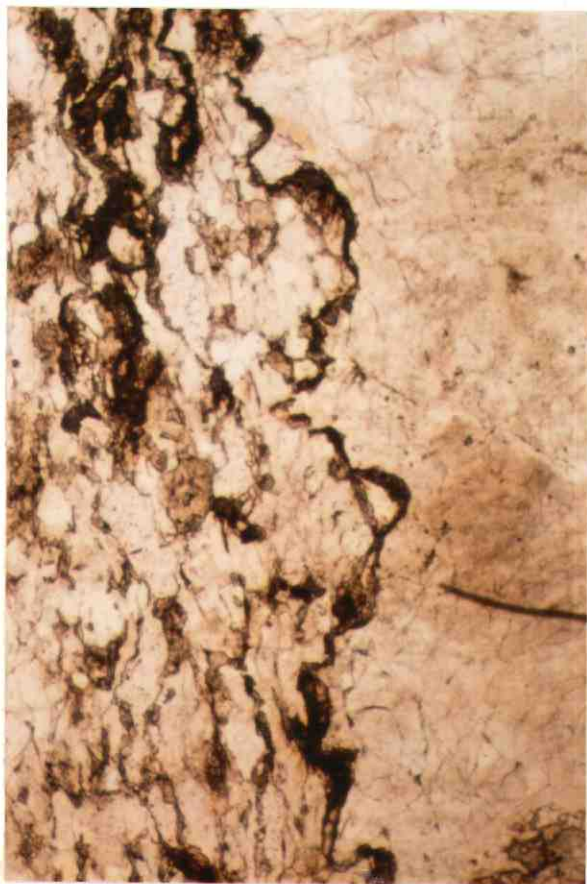


Figure 6c



Figure 6d

Figure 7. Photomicrographs of fluid inclusions, fractures, and microstylolites in schist from the Traenabanken 6609/7-1 well.

- a) Trains of fluid inclusions cross-cutting the metamorphic fabric. The foliation parallels the long dimension of the photo. The more strongly developed set of fluid inclusions is at high angles to the foliation. Another set parallels the foliation. (Cross-polarized light; long dimension of photo is 0.8mm; Core 2, Cut C, section 2).
- b) Two sets of fluid conclusion trains, one parallel to metamorphic foliation (long dimension of photo), the second at 60° to this. (Cross-polarized light; long dimension of photo 0.8mm; Core 2, Cut C, section 2.)
- c) A discontinuous fracture following a zone of fluid inclusions, both inclined at 60° to the metamorphic foliation. Foliation is at a slight angle to the short dimension of the photo. The dark streaking is due to numerous trains of fluid inclusions. The fluid inclusion trains occur at 60° to the fracture. (Plane light; short dimension of photo is 1.6mm; Core 1, Cut C, section 5.)
- d) A swarm of microstylolites oriented subparallel to the metamorphic foliation. Dark streaking is due to fluid inclusion trains that are at $80-90^{\circ}$ to the microstylolites. (Plane light; short dimension of the photo is 1.6mm; Core 1, Cut C, section 5.)

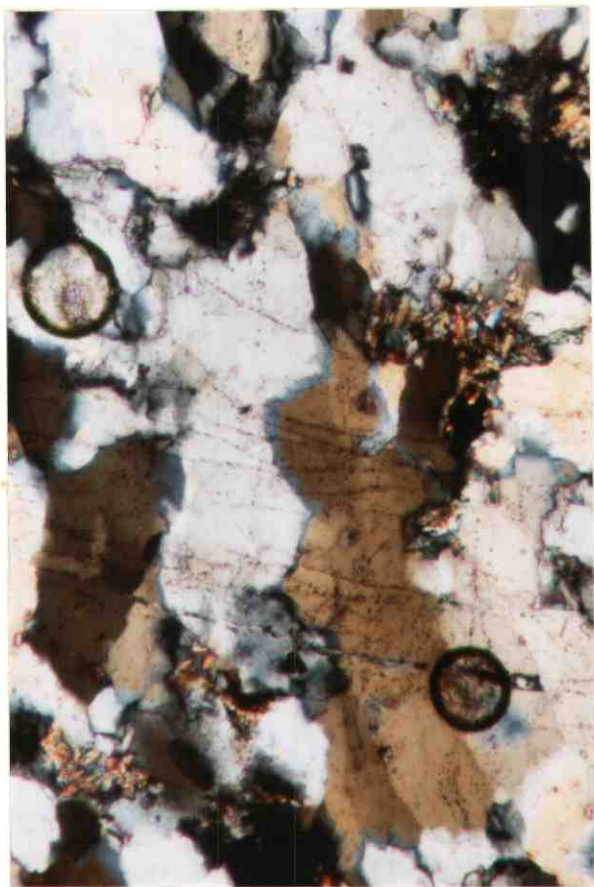


Figure 7a

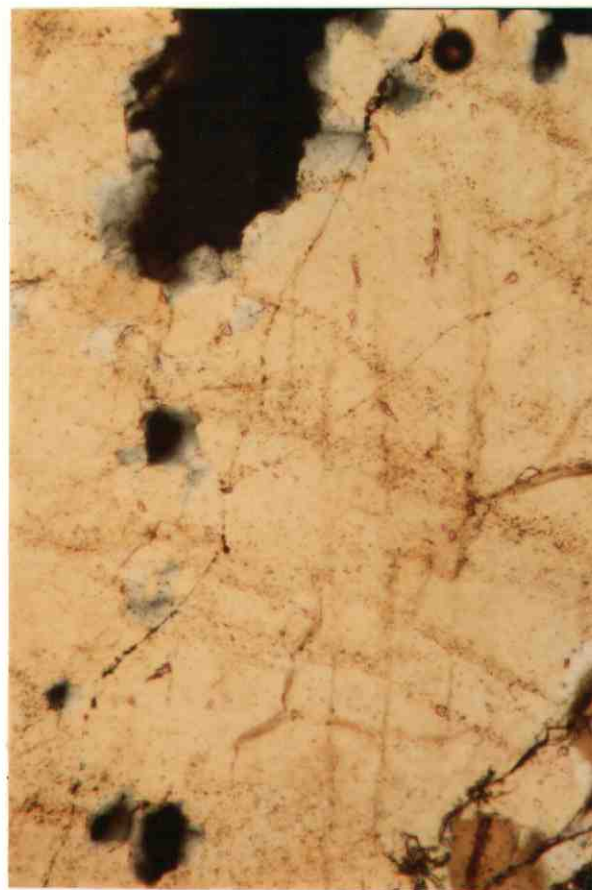


Figure 7b



Figure 7c

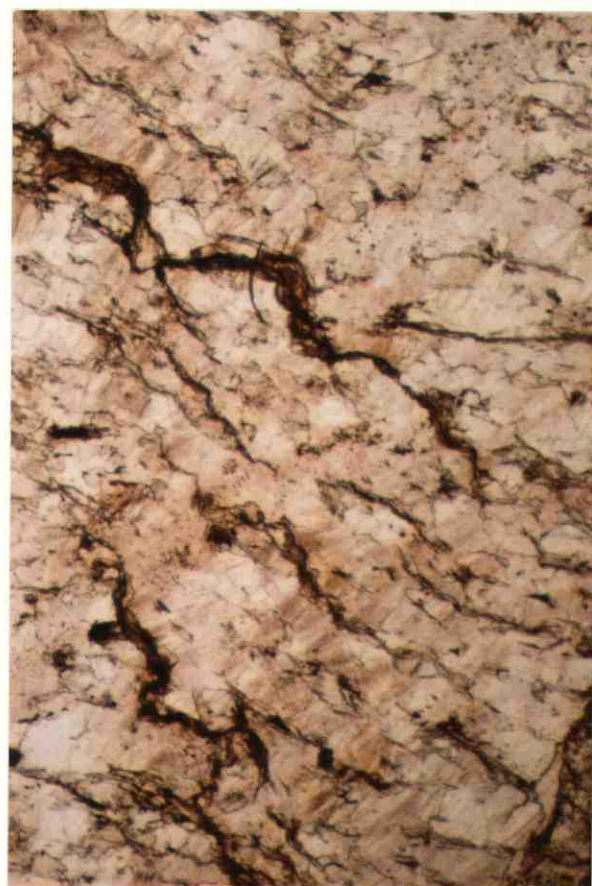


Figure 7d

January 16, 1984

FILE: BNP-2-84

WSS-1-84

RKC-2-84

A-15

Figure 8. Schematic summary of Phase 2 structures in schist from the Traenabanken 6609/7-1 well. A, B, and C are fractures, wavy lines at D, E, and F are microstylolites, and dots represent trains of fluid inclusions.

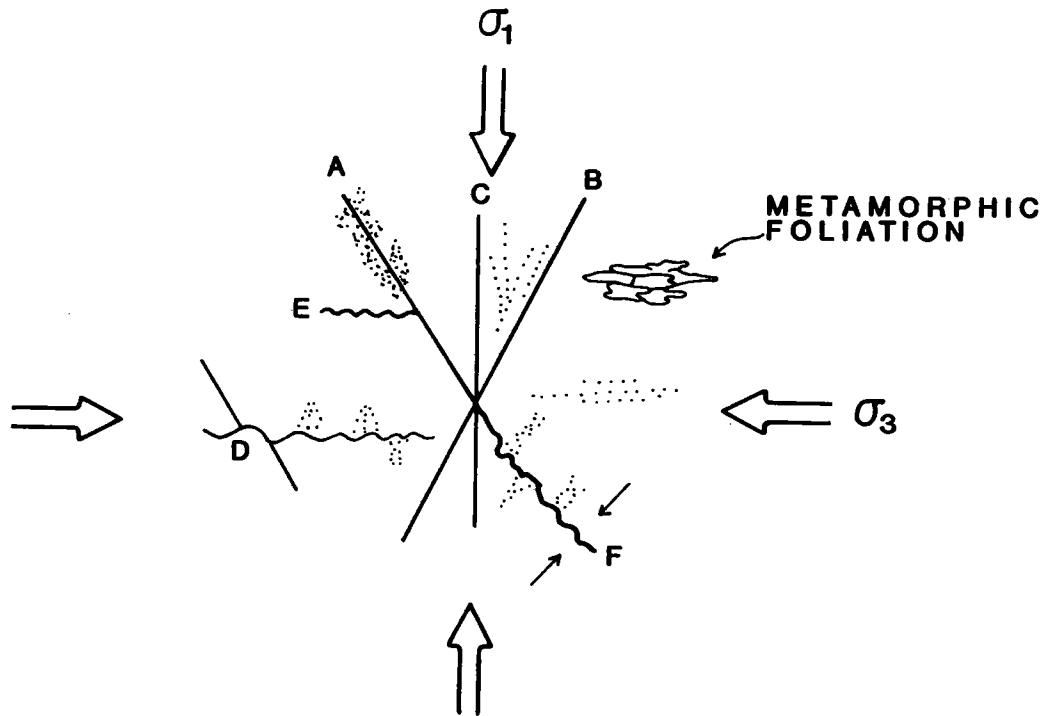


Figure 8

Figure 9. Photomicrographs of calcite veins in schist from the Traenabanken 6609/7-1 well.

- a) Portion of the calcite vein shown in Figure 5; the metamorphic wall rock is on the right. An early, highly twinned, generation of calcite is in the right-center and a second generation of calcite is on the left. (Cross-polarized light; long dimension of photo is 2.3mm; Core 1, Cut A, section 3.)
- b) Another portion of the same calcite vein. Note the breccia separating the two generations of calcite. Breccia fragments are calcite. (Long dimension of photo is 2.3mm; Core 1, Cut A, section 3; plane light.)
- c) A conjugate set of calcite veins. The metamorphic foliation is at a slight angle to the short dimension of the photo. The dark streaking is due to trains of fluid inclusions that parallel the discontinuous calcite vein. (Short dimension of photo is 4.1mm; Core 2, Cut C, section 2; plane light.)

Figure 9a



Figure 9b

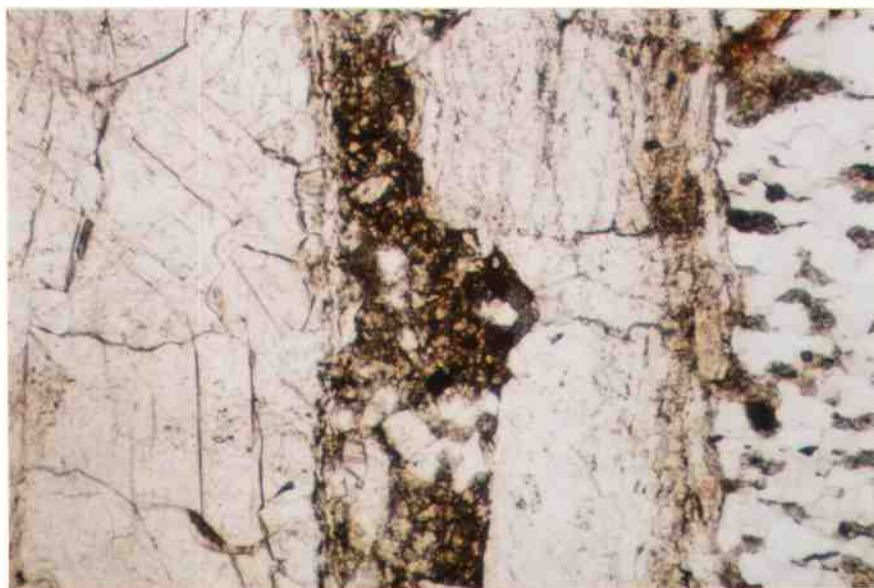


Figure 9c

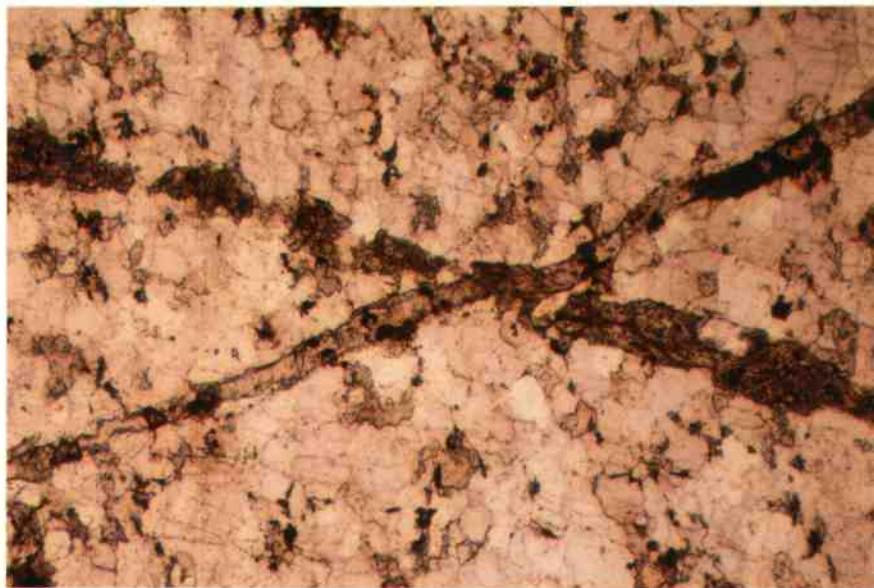


Figure 10. Photomicrographs of dilation breccias from the Traenabanken 6609/7-1 well.

- a) Dilation breccia, with clasts of broken wallrock (schist), variably rotated, cemented by sparry calcite. Margin of breccia zone follows pre-existing fractures. (Core 1, Cut C, section 5; plane light; short dimension of photo is 12mm.)
- b) A portion of the breccia in a; metamorphic wallrock is on the right. The rock clasts are rotated. (Long dimension of photo is 6mm; Core 1, Cut C, section 5; cross-polarized light.)
- c) The edge of the breccia zone in a. Breccia is on the top. The fracture cuts the wallrock into a fragment that would have eventually broken off and been incorporated into the breccia. (Short dimension of photo is 4mm; Core 1, Cut C, section 5; plane light.)

Figure 10a



Figure 10b

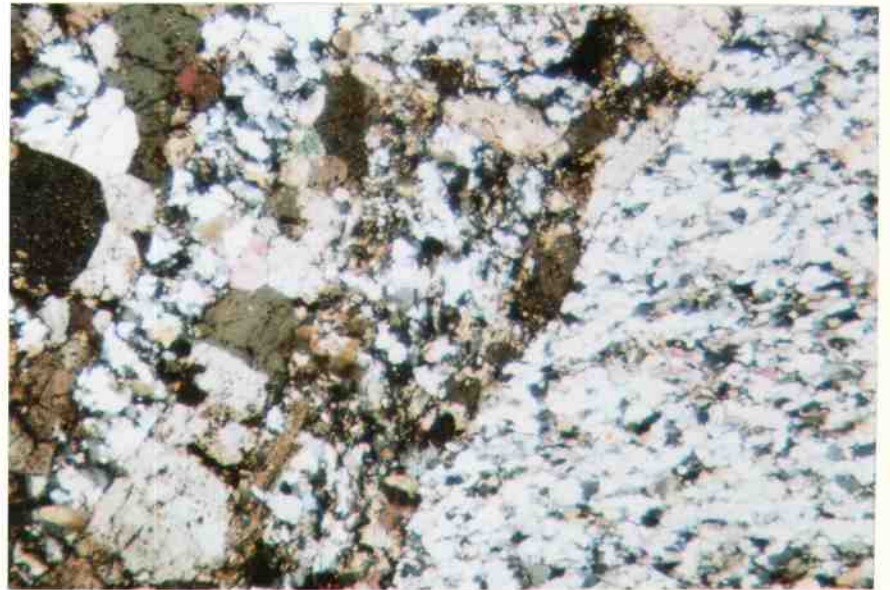


Figure 10c

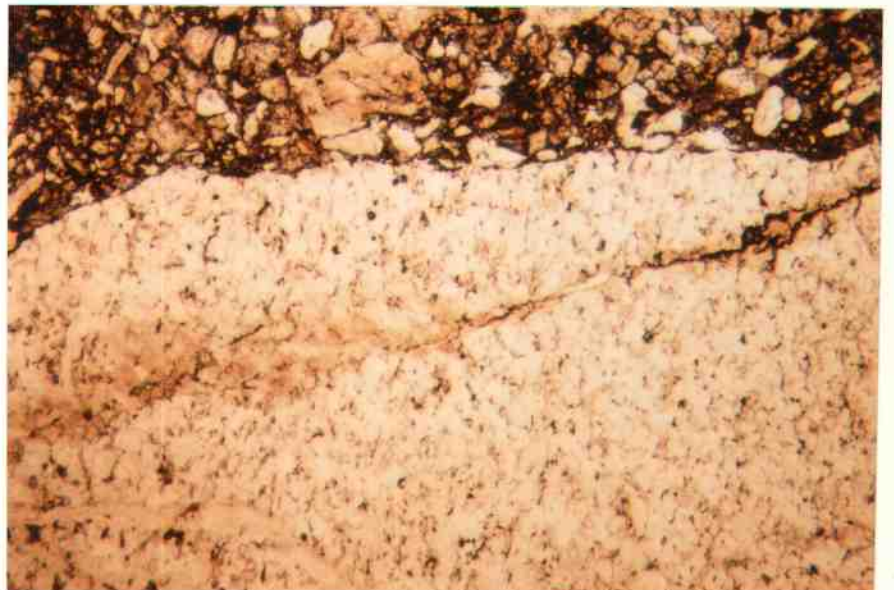


Figure 11. Photographs of the tectonic breccia from the top of Core 1, Traenbanken 6609/7-1 well, at 1944.24m.

- a) Fragments in the core are angular and show various stages of disaggregation. Narrow zones of finely comminuted rock separate many of the fragments.
- b) Closer view of the upper portion of a. Chlorite (?) and/or epidote probably impart the color to the greenish zones which cross-cut the entire core.
- c) Photo of the surface of one of the finely-comminuted zones that cross-cut the core. Slickensides trend vertically in the photo and indicate that these are fault zones.

Figure 11a



Figure 11b



Figure 11c



January 16, 1984

FILE: BNP-2-84

WSS-1-84

RKC-2-84

A-23

Figure 12. Secondary inclusions in matrix quartz. Linear "trains" of minute, 2 phase, liquid-vapor fluid inclusions in quartz are related to microfracturing during deformational Phase 2. Both photos were taken at 400X magnification. (Narrow dimension of each photograph is 38 μm .)



Figure 12a



Figure 12b

Figure 13. Vein calcite related to phase 3 structural deformation.

- a) 50X magnification. Note the clear, Type 2 calcite in the center of the photo surrounded by the very dark, mottled, Type 1 calcite. The dark "boot-shaped" inclusion near the center of the photo may contain hydrocarbon liquid. Narrow dimension of photo is 300 μm . Figure 14 shows a higher magnification view of this inclusion.
- b) 200X magnification. A close-up of a fluid inclusion in Type 1 calcite (dark zone, center of photo). The vapor bubble is about 4 μm in diameter.
- c) 200X magnification. A close-up of irregularly shaped fluid inclusions in Type 2 vein calcite. The vapor bubble in the large inclusion to the upper left of center is about 5 μm across.

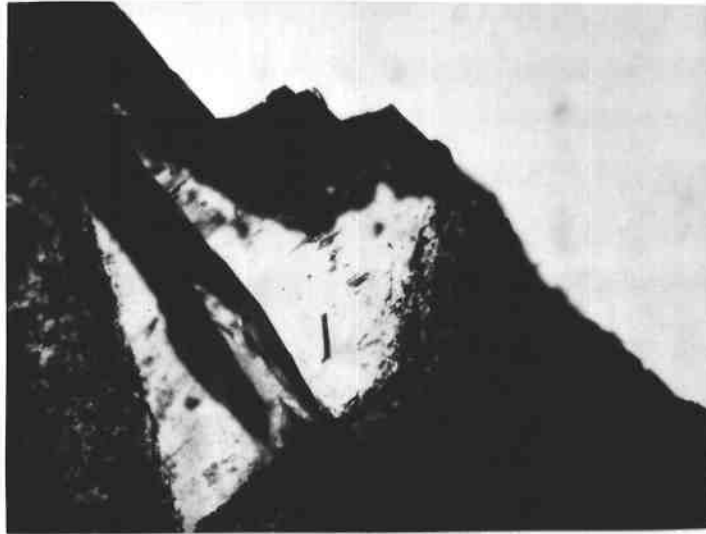


Figure 13a



Figure 13b

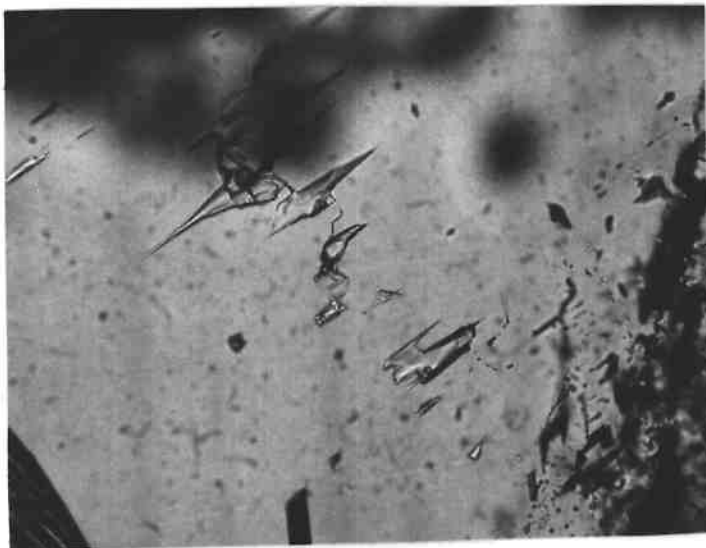


Figure 13c

Figure 14. Liquid hydrocarbon(?) -bearing inclusion in Type 2 vein calcite.

- a) 200X magnification. Note the curved surface of the dark material in the inclusion. The inclusion is about 10 μm in width. This photo was taken at room temperature before the sample was heated to 130 $^{\circ}\text{C}$.
- b) 200X magnification. Note the disappearance of the curved phase boundary. This photo was taken at room temperature after the sample was heated to 130 $^{\circ}\text{C}$.



Figure 14a



Figure 14b

TABLE 1. Compositional range and average of all 48 feldspar analyses from Cores 1 and 2, Traenabanken 6609/7-1 well; microprobe analyses in wt. % except as noted at bottom of table. Wt. % values are shown to only significant figures and analytical uncertainty lies in the last decimal shown for each oxide.

	<u>Range</u>		<u>Average</u>
	<u>Lowest</u>	<u>Highest</u>	
SiO ₂	62.5	64.8	63.9
Al ₂ O ₃	19.0	19.9	19.4
TiO ₂	0.00	0.05	0.00
"FeO"	0.00	0.12	0.00
MgO	0.00	0.04	0.00
CaO	0.00	0.08	0.01
K ₂ O	15.4	16.6	16.0
Na ₂ O	0.16	1.40	<u>0.64</u>
Sum	98.3(4)	101.3(9)	99.9(7)
		<u>Mol. %</u>	
Or	88.06	98.27	94.24
Ab	1.50	11.78	5.70
An	0.00	0.38	0.06

TABLE 2. Compositional ranges and averages of muscovite analyses from Cores 1 and 2. Traenabanken 6609/7-1 well; microprobe analyses in wt. % are shown to only significant figures and analytical uncertainty lies in the last decimal shown for each oxide. The minimum K₂O value for all analyses is atypically low because of intergrown kaolinite (K₂O-free) in that analysis. The range of K₂O in kaolinite-free muscovites is much narrower as indicated in the separate listing in the table. The low sums reflect the 3-4.5 percent H₂O typically present in muscovite.

	<u>All Analyses</u>			<u>No Intergrown Kaolinite</u>		
	<u>Range</u>		<u>Average</u>	<u>Range</u>		<u>Average</u>
	<u>Lowest</u>	<u>Highest</u>		<u>Lowest</u>	<u>Highest</u>	
SiO ₂	44.5	49.1	46.0	44.5	48.9	45.8
Al ₂ O ₃	32.2	40.6	35.4	33.2	37.8	35.0
TiO ₂	0.00	1.47	0.57	0.00	1.47	0.61
"FeO"	0.30	3.24	1.73	0.82	3.15	1.88
MgO	0.03	1.76	0.85	0.17	1.66	0.93
CaO	0.00	0.45	0.04	0.00	0.21	0.03
K ₂ O	6.85	11.3	10.6	9.96	11.2	10.8
Na ₂ O	0.07	0.59	<u>0.28</u>	0.08	0.59	<u>0.32</u>
Sum	93.0(7)	98.5(5)	95.4(7)	93.0(7)	98.5(5)	95.3(1)
No. of Anal.			79			57

TABLE 3. Average compositions of feldspars in different thin sections of core samples from the Traenabanken 6609/7-1 well. Data are microprobe analyses in wt. % except where indicated at the bottom of the table. The magnitude of the analytical uncertainty for an individual analysis is indicated by the use of only significant figures for the tabulated average oxide compositions. End-member compositions in mol. % at the bottom of the table are carried to two decimals to allow for tabulation of the low An values. The average of all analyses is shown for comparison. Sample numbers listed at the top of the table give Core No./Cut/Section No.

Sample	<u>1/A/1</u>	<u>1/A/3</u>	<u>1/C/1</u>	<u>1/C/2</u>	<u>1/C/4</u>	<u>1/C/5</u>	<u>1/C/7</u>	<u>2/C/1</u>	All Analyses
SiO ₂	63.8	64.5	63.8	64.1	63.8	63.8	64.0	63.4	63.9
Al ₂ O ₃	19.5	19.4	19.6	19.5	19.3	19.6	19.5	19.2	19.4
TiO ₂	0.01	0.00	0.00	0.00	0.00	0.01	0.01	n.d.	0.00
"FeO"	0.03	0.06	0.00	0.01	0.01	0.01	0.03	0.02	0.02
MgO	0.00	0.00	0.00	0.00	0.00	0.00	0.00	n.d.	0.00
CaO	0.01	0.01	0.02	0.02	0.02	0.03	0.01	0.00	0.01
K ₂ O	15.9	15.8	16.4	16.1	16.0	15.9	15.9	16.2	16.0
Na ₂ O	<u>0.84</u>	<u>0.87</u>	<u>0.87</u>	<u>0.54</u>	<u>0.30</u>	<u>0.62</u>	<u>0.80</u>	<u>0.30</u>	<u>0.64</u>
Sum	100.0(9)	100.6(4)	100.8(0)	100.2(7)	99.4(3)	99.9(7)	100.2(5)	99.1(2)	99.9(7)
MOL. %									
Or	92.56	92.29	92.53	95.09	97.13	94.24	92.93	97.26	92.24
Ab	7.42	7.66	7.42	4.81	2.76	5.59	7.02	2.74	5.70
An	0.02	0.05	0.05	0.10	0.11	0.17	0.05	0.00	0.06
No. of Anal.	6	3	4	6	3	5	13	8	49

TABLE 4. Average compositions of muscovite in different thin sections of core samples from the Traenabanken 6609/7-1 well. Data are microprobe analyses in wt. %. The magnitude of the analytical uncertainty for an individual analysis is indicated by the use of only significant figures for the tabulated average oxide compositions. In this table all muscovite analyses from a given thin section are included in the listed averages, with no distinction made between muscovites intergrown with kaolinite and those kaolinite-free. (See Table 2 and text.) The low sums of the analyses reflect the 3-4.5% H₂O typically present in muscovite. The average of all analyses is shown for comparison. Sample numbers listed at the top of the table give Core No./Cut/Section No.

<u>Sample</u>	<u>1/A/1</u>	<u>1/A/3</u>	<u>1/C/1</u>	<u>1/C/2</u>	<u>1/C/4</u>	<u>1/C/5</u>	<u>1/C/7</u>	<u>2/C/1</u>	<u>All Analysis</u>
SiO ₂	45.4	46.2	47.3	46.4	46.3	45.9	46.4	45.3	46.0
Al ₂ O ₃	34.6	34.7	35.1	37.3	35.4	36.7	34.0	35.0	35.4
TiO ₂	1.15	1.14	1.15	0.21	0.36	0.26	0.98	0.24	0.57
"FeO"	1.45	1.56	1.51	1.41	1.48	1.46	1.69	2.33	1.73
MgO	1.05	1.14	1.09	0.46	0.87	0.51	1.18	0.83	0.85
CaO	0.04	0.06	0.03	0.04	0.03	0.07	0.01	0.02	0.04
K ₂ O	10.8	10.5	9.62	9.95	10.8	10.9	10.2	10.9	10.6
Na ₂ O	<u>0.45</u>	<u>0.39</u>	<u>0.29</u>	<u>0.15</u>	<u>0.30</u>	<u>0.25</u>	<u>0.33</u>	<u>0.26</u>	<u>0.28</u>
Sum	95.0(4)	95.6(9)	96.0(9)	95.9(2)	95.5(4)	96.0(5)	94.7(9)	94.8(8)	95.4(7)
No. of Anal.	7	10	6	10	7	11	5	23	79

TABLE 5. Traenabanken muscovite compositions compared to muscovites from other metamorphic terranes. For microprobe analyses (Traenabanken) all Fe is calculated as "FeO".

	Traenabanken Lowest-SiO ₂ Muscovite ¹	Traenabanken Highest-SiO ₂ Muscovite ²	Traenabanken Average Muscovite ³	"Ideal" Muscovite ⁴	Muscovite, Garnet-Mica Schist ⁵	Phengitic Muscovite, Greenschist ⁶
SiO ₂	44.5	49.1	46.0	45.26	46.17	48.98
Al ₂ O ₃	34.6	32.2	35.4	38.40	33.85	25.05
TiO ₂	0.16	1.05	0.57		1.07	
Fe ₂ O ₃					0.99	5.74
FeO					0.99	1.72
"FeO"	2.42	1.90	1.73		(1.88)	(6.37)
MgO	1.04	1.76	0.85		1.44	2.90
CaO	0.00	0.01	0.04			
K ₂ O	11.0	10.2	10.6	11.82	9.60	11.29
Na ₂ O	0.25	0.23	0.28		1.08	
H ₂ O ⁺	<u>(4.52)*</u>	<u>(3.55)*</u>	<u>(4.52)*</u>	<u>4.52</u>	<u>4.52</u>	<u>4.32</u>
Sum	(98.49)*	(100.00)*	(99.99)*	100.00	99.71	100.00

Cations on the basis of 24 (O,OH,F)

Si	6.0600	6.5652	6.1252	6.0000	6.151	6.6800
Al	1.9400	1.4348	1.8748	2.0000	1.849	1.3200
Al	3.6126	3.6401	3.6815	4.0000	3.467	2.6975
Ti	0.0164	0.1052	0.0568	---	0.107	---
Fe ⁺³	---	---	---	---	0.100	0.5882
Fe ⁺²	0.2757	0.2121	0.1928	---	0.110	0.1958
Mg	0.2111	0.3503	0.1688	---	0.285	0.5890
Ca	---	0.0016	0.0056	---	---	---
K	1.9114	1.7404	1.8004	2.0000	1.632	1.9662
Na	0.0654	0.0594	0.0720	---	0.278	---
OH	(4.0862)	(3.1658)	(3.9960)	4.0000	4.018	3.9274

(Footnotes on following page)

(Table 5 Cont., Footnotes)

Notes on Analyses:

1. Analysis No. 21, sample 2/C/1: represents lowest-silica muscovite analyzed in Traenabanken samples.
 2. Analysis No. 11, sample 1/A/3: represents highest-silica muscovite analyzed in Traenabanken samples
 3. Average of all Traenabanken muscovite analyses.
 4. Composition calculated from stoichiometric formula $K_2Al_4[Si_6Al_2O_{20}](OH)_4$.
 5. Muscovite from medium-grade garnet mica schist, Morar, Inverness-shire, Scotland: analysis No. 14, Table 5, vol. 3, Deer et al . (1962).
 6. Composition calculated from formula given for average muscovite in Otago, N.Z., greenschists, by Turner (1968), p. 274. The formula: $K_2Mg_{0.6}Fe^{2+}_{0.2}Al_{2.9}(Al_{1.2}Si_{6.8}O_{20})(OH)_4$.
- * For the purpose of calculating the structural formula for Traenabanken microprobe analyses to compare to other data in the table, an amount of H₂O was added up to the maximum of 4.52% (for ideal muscovite); in one case a lower value was used to keep the adjusted sum at 100%.

January 16, 1984
FILE: BNP-2-84
WSS-1-84
RKC-2-84

REFERENCES CITED

Deer, W. A., Howie, R. A., and Zussman, J. (1962) Rock Forming Minerals, vol. 3, John Wiley and Sons, N.Y., 270 pp.

Greenwood, H. J. (1976) Metamorphism at moderate temperatures and pressures, in Bailey, D.K. and MacDonald, R., eds., The Evolution of the Crystalline Rocks, Academic Press, N.Y., p. 187-259.

Turner, F. J. (1968) Metamorphic Petrology, McGraw-Hill, N.Y., 403 pp.